Peculiarities of the Dynamics of Incommensurate Superstructures in Crystals of the $[N(CH_3)_4]_2MeCl_4$ Family with Factor $n = 3$

S. Sveleba[a], I. Katerynchuk[a], Y. Shmygelskyi[a], I. Kunyo[a] and V. Kotsun[b]

[a] *Department of Optoelectronics and Information Technologies Ivan Franko National University of Lviv, 107 Tarnavskoho Str., Lviv 79017, Ukraine*
[b] *Lviv Branch of Private Higher Education Establishment "European University", 5 Kushevych Str., Lviv 79019, Ukraine*

Received: 31.08.2025 & Accepted: 01.06.2026

Doi: 10.12693/APhysPolA.149.124

*e-mail: incomlviv@gmail.com

This study investigates the dynamics of incommensurate superstructures in crystals of the $(N(CH_3)_4)_2MeCl_4$ family with a unit-cell multiplication factor $n = 3$ using numerical simulations within the Landau–Ginzburg framework. The incommensurate phase is described by a two-component order parameter with modulation induced by the Lifshitz invariant and analyzed using Fourier spectra, Lyapunov exponents, dynamic-regime maps, and modulation wave-vector evolution. The results reveal the existence of two structurally distinct incommensurate states within a single incommensurate phase. The first regime corresponds to sinusoidal modulation with narrow periodicity windows and localized chaotic behavior, whereas the second regime exhibits solitonic and stochastic dynamics characterized by higher harmonics, broad periodicity distributions, and hyperchaotic states. The transition between these regimes occurs near the control parameter $K \approx 0.4$, where additional modulation harmonics emerge. For $K > 1.2$, the system enters a hyperchaotic regime with two positive Lyapunov exponents. The role of surface energy is shown to be essential for phase stability. Its increase modifies the effective anisotropic interaction, shifts the phase-transition temperatures, narrows the stability interval of the incommensurate phase, and induces transformations between distinct incommensurate structures through an intermediate commensurate phase. The physical significance of the case $n = 3$ is connected with the tripling of the unit cell and the emergence of threefold anisotropy in the thermodynamic potential, which determines the sequence of phase transitions and lock-in behavior. The obtained results provide a consistent physical interpretation of modulation dynamics in low-symmetry ferroelastic crystals and establish a framework for the analysis of complex incommensurate phases.

topics: incommensurate superstructure, Lyapunov exponents, dynamic-regime maps, modulation wave vector

1. Introduction

Incommensurate superstructures serve as model systems for studying nonlinear dynamics, deterministic chaos, and self-organization processes in condensed matter physics. Particularly important representatives of such systems are dielectric crystals of the A_2BX_4 family, which exhibit complex sequences of structural phase transitions involving commensurate, incommensurate, long-period, and chaotic phases. The diversity of these phase states stems primarily from the existence of different dynamical regimes of the incommensurate (IC) structure, namely sinusoidal, solitonic, and stochastic regimes.

Crystals of the $[N(CH_3)_4]_2MeCl_4$ family (where Me = Zn, Cu, Co, Fe) belong to this class of compounds and demonstrate a wide variety of modulated states associated with ferroelastic and incommensurate phase transitions. These materials exhibit a transition to an IC phase with nanoperiodicity, where the modulation period is typically within the range of 100–160 nm [1]. The coexistence of long-period commensurate and incommensurate phases makes these systems highly suitable for studying dynamic-regime maps and the evolution of complex modulated structures.

A representative example is the crystal $(N(CH_3)_4)_2CuCl_4$, which in the ferroelastic phase exhibits unit-cell multiplication with factor $n = 3$. This tripling of the unit cell determines the symmetry of the thermodynamic potential and strongly influences the formation of lock-in states and the stability of the IC phase.

The integer parameter n defines the multiplication factor of the unit cell and determines the anisotropic symmetry of the free-energy potential. For $n = 3$, the thermodynamic potential acquires a threefold anisotropy represented by the term $\cos(n\varphi)$, where φ is the phase of the IC modulation. Physically, this term describes the stabilization of commensurate states and governs the transitions between sinusoidal, solitonic, and stochastic regimes of the IC superstructure.

The IC phase is described using a two-component order parameter (η_1, η_2), which corresponds to two symmetry-related components of the structural distortion associated with the displacement of tetrahedral groups and local ferroelastic distortions. In complex notation, the order parameter is written as $\eta = \eta_1 + \mathrm{i}\eta_2$, while in polar representation it takes the form $\eta_1 = \eta\cos(\varphi)$, $\eta_2 = \eta\sin(\varphi)$, where η is the amplitude of the modulation wave, and φ is its phase. The amplitude η characterizes the strength of the structural modulation, whereas φ determines the spatial evolution of the IC wave.

The modulation wave vector q characterizes the spatial periodicity of the IC structure and determines the modulation wavelength according to $L = 2\pi/q$. Its temperature dependence $q(T)$ reflects the evolution of the modulation period during transitions between the parent, incommensurate, and commensurate phases.

At the IC transition temperature $T_i = 297$ K, an incommensurate superstructure appears at a special point of the Brillouin zone (m/n, where $n = 3$ and $m = 1$), with modulation wave vector $q = (\frac{1}{3} - \delta)/c$. The variation of δ is relatively small ($\delta \approx 0.0075$–0.007), resulting in a modulation wavelength near T_i of approximately $L_i \approx 1617$ Å [1]. Upon further cooling toward the commensurate ferroelastic phase transition ($T_c = 291$ K), the system undergoes an increase in anisotropic interaction described by the Dzyaloshinskii invariant and quantified by the parameter K [1].

The statement that the crystal $(\mathrm{N(CH_3)_4})_2\mathrm{CuCl_4}$ represents a model system with a well-developed IC phase is supported by extensive experimental and theoretical evidence. X-ray diffraction studies [1] revealed the appearance of temperature-dependent satellite reflections, which provide direct evidence of incommensurate modulation. Raman and infrared spectroscopy investigations [2] demonstrated phonon-mode splitting, the emergence of new modulation-induced modes, and a reduction of crystal symmetry within the IC phase.

The Landau formalism, including fourth-order spatial derivatives and the Dzyaloshinskii invariant, successfully describes the emergence of the IC phase, the temperature dependence of the modulation wave vector $q(T)$, lock-in effects, and the occurrence of solitonic and chaotic solutions [3]. Numerical modeling also confirms the existence of stable modulated solutions within realistic temperature intervals [4]. In particular, the numerical integration of Landau–Ginzburg-type differential equations demonstrates the stability of these solutions under variations of temperature and anisotropic interaction parameters. Thus, the crystal $(\mathrm{N(CH_3)_4})_2\mathrm{CuCl_4}$ can be considered a reference system for studying IC superstructures.

The validity of stable modulated solutions is confirmed within both microscopic and phenomenological theoretical approaches. The microscopic theory explains modulation through atomic-level interactions. The system is modeled as a chain of interacting particles with local anisotropies. The microscopic origins of modulation include anisotropic interactions between $\mathrm{CuCl_4^{2-}}$ layers, coupling between local dipoles or atomic displacements, and Jahn–Teller effects associated with $\mathrm{Cu^{2+}}$ ions (d^9 configuration), which induce local lattice distortions. Numerical models based on molecular dynamics, Monte Carlo simulations, and finite-difference methods show that within the temperature interval $T \in [T_{c2}, T_{c1}]$, energy minimization favors modulated structures over homogeneous phases. These stable solutions exhibit distinct periodicities consistent with the experimentally observed dependence $q(T)$ [1, 5, 6].

The phenomenological Landau theory with a two-component order parameter provides a macroscopic description through the free-energy functional

$$F = \int \mathrm{d}x \left[\frac{r}{2}(\eta_1^2 + \eta_2^2) + \frac{u}{4}(\eta_1^2 + \eta_2^2)^2 + \frac{v}{2}\left(\frac{\mathrm{d}\eta_1}{\mathrm{d}x}\right)^2 + \frac{v}{2}\left(\frac{\mathrm{d}\eta_2}{\mathrm{d}x}\right)^2 + \frac{w}{2}\left(\frac{\mathrm{d}^2\eta_1}{\mathrm{d}x^2}\right)^2 + \frac{w}{2}\left(\frac{\mathrm{d}^2\eta_2}{\mathrm{d}x^2}\right)^2 + \sigma\Big(\eta_1\frac{\mathrm{d}\eta_2}{\mathrm{d}x} - \eta_2\frac{\mathrm{d}\eta_1}{\mathrm{d}x}\Big)\right], \tag{1}$$

where $r = \alpha\,(T - T_c)$ and $\sigma = K$. Here, σ represents the Dzyaloshinskii invariant responsible for modulation asymmetry and incommensurability.

The numerical analysis leads to a system of two coupled fourth-order differential equations. An initial approximation of the form $\eta_1(x) = A\cos(qx)$, $\eta_2(x) = A\sin(qx)$ is introduced. Iterative numerical solutions yield stable quasiperiodic profiles minimizing the free-energy functional. The resulting temperature evolution of $q(T)$ agrees well with experimental observations [3, 4].

In both microscopic and phenomenological approaches, numerical modeling confirms that modulated solutions exist and remain stable within physically relevant temperature intervals. The temperature dependence of $q(T)$ is reproduced as a consequence of modulation-period stabilization. The spatial structure $\eta(x)$ reflects sinusoidal, solitonic, and quantized waveforms that correspond to experimentally observed modulated states in $\mathrm{CuCl_4}$-based crystals.

Therefore, numerical modeling provides a reliable tool for predicting and explaining the nature of incommensurate superstructures in $(N(CH_3)_4)_2CuCl_4$.

The aim of this work is to perform numerical modeling of the dynamics of the incommensurate superstructure for $n = 3$ within the Landau–Ginzburg formalism and to analyze the evolution of Fourier spectra, Lyapunov exponents, dynamic-regime maps, and the modulation wave vector under the influence of anisotropic interaction, long-range interaction, and surface energy.

2. Materials and methods

The phenomenological description of the incommensurate (IC) phase is based on the Landau free-energy functional with a two-component order parameter. The Lifshitz invariant is responsible for the appearance of incommensurability and enables spatial modulation of the order parameter. The two-component order parameter is written in polar coordinates as $\eta_1 = \eta\cos(\varphi)$, $\eta_2 = \eta\sin(\varphi)$, where η is the amplitude of the modulation wave, and φ is its phase. Physically, η describes the strength of the structural modulation, while φ determines the spatial evolution of the IC wave and its lock-in behavior.

In this representation, the free-energy functional takes the form

$$\Phi = \int \mathrm{d}z \,\Big[-r\,\eta^2 + u\,\eta^4 + a\,\eta^2\Big(1+\cos(n\varphi)\Big) - \sigma\eta^2\frac{\partial\varphi}{\partial z} + \frac{\gamma}{4}\Big(\Big(\frac{\partial\eta}{\partial z}\Big)^2 + \eta^2\Big(\frac{\partial\varphi}{\partial z}\Big)^2\Big)\Big] + \beta\Big[\Big(\frac{\partial^2\eta}{\partial z^2} - \eta\Big(\frac{\partial\varphi}{\partial z}\Big)^2\Big)^2 + \Big(2\frac{\partial\eta}{\partial z}\frac{\partial\varphi}{\partial z} + \eta\frac{\partial^2\varphi}{\partial z^2}\Big)^2\Big]. \tag{2}$$

The term $\cos(n\varphi)$ describes the anisotropic symmetry of the thermodynamic potential and determines the stabilization of commensurate states. For the present case, $n = 3$ corresponds to the tripling of the unit cell and results in a threefold anisotropy of the free-energy landscape. The Lifshitz invariant term $\sigma\,\eta^2(\partial\varphi/\partial z)$ introduces asymmetry of modulation and is responsible for the existence of the IC phase.

To simplify the numerical treatment, the following dimensionless variables were introduced $\eta = \sqrt{r/(2u)}\;R$, $z = \sqrt{\gamma/r}\;\xi$, where $R = R(\xi)$ is the dimensionless amplitude of the order parameter, and ξ is the dimensionless spatial coordinate.

Taking into account the contribution of the surface energy, the free-energy functional (2) transforms into

$$\Phi = \int \mathrm{d}\xi\;\frac{r^2}{2u}\Big[-R^2 + \frac{1}{2}R^4 + \frac{\omega r}{2u}R^2\Big(1+\cos(n\varphi)\Big) - \frac{\sigma}{\sqrt{r\gamma}}R^2\varphi' + (R')^2 + R^2(\varphi')^2 + \frac{\beta r}{\gamma} \times \Big[\Big(R'' - R(\varphi')^2\Big)^2 + \Big(2R'\varphi' + R\varphi''\Big)^2\Big]\Big] - \frac{\alpha\sigma}{4u}R^2. \tag{3}$$

Here, $R' = \partial R/\partial\xi$, $R'' = \partial^2 R/\partial\xi^2$, and $\varphi' = \partial\varphi/\partial\xi$, $\varphi'' = \partial^2\varphi/\partial\xi^2$. The parameter u characterizes the strength of isotropic interactions, while ω determines the strength of anisotropic interactions.

The surface-energy contribution describes finite-size effects and boundary-induced distortions. Physically, it modifies the amplitude of the order parameter near the crystal surface and induces a phase shift of the modulation wave. As a result, the stability interval of the IC phase changes, and transitions between distinct IC structures may occur through an intermediate commensurate phase.

The variation of the free-energy functional (3) yields a system of two coupled nonlinear differential equations for the amplitude and phase functions, respectively,

$$R'' - R^3 + \big(1 - (\varphi')^2 + T\varphi'\big)\,R - R^{n-1}K \times \big(\cos(n\varphi) + 1\big) = 0 \tag{4}$$

and

$$\varphi'' + \frac{2R'}{R}\Big(\varphi' - \frac{T}{2}\Big) + R^{n-2}K\sin(n\varphi) = 0, \tag{5}$$

where $T = \sigma/\sqrt{\gamma r}$, $K = 2^{n/2}r^{n/2}\,n\,\omega\,u^{1-n/2}$. Both T and K are dimensionless control parameters. The parameter T reflects the contribution of long-range interactions, while K describes the strength of anisotropic interactions (related to the Dzyaloshinskii–Lifshitz mechanism) and governs the transition between sinusoidal, solitonic, and stochastic regimes.

The resulting system of coupled nonlinear differential equations for the amplitude R and phase φ was solved numerically using the BDF (Backward Differentiation Formula) method implemented in the Python environment with the SciPy library. This method is particularly suitable for stiff nonlinear differential systems and ensures stable convergence for strongly nonlinear solutions.

Lyapunov exponents were calculated using the JiTCODE and SciPy libraries according to the standard Benettin algorithm [7]. The Lyapunov spectrum allows identification of periodic, quasiperiodic, chaotic, and hyperchaotic regimes. The presence of one positive exponent corresponds to a strange attractor, while two positive exponents indicate hyperchaotic dynamics.

The value of the modulation wave vector q of the IC superstructure was obtained from the spatial variation of the amplitude of the order parameter and from Fourier analysis of the modulation profile. The selected boundary conditions correspond to the minimization of the free-energy functional in a finite crystal with symmetric surfaces. Their physical meaning is to ensure equilibrium between bulk modulation and surface-induced distortions while avoiding artificial external forces at the crystal boundaries.

Together with the boundary conditions $R'''=0$, $R''=0$, $\varphi'=0$, $(\varphi'')'=0$, the variation of the free-energy functional leads to the following dimensionless equation for the phase function

$$\varphi'\left[1-\frac{1}{2}\left(\frac{R'}{R}\right)^2+(\varphi')^2\right]+\frac{R'}{R}(\varphi'-T)+KR^{n-2}\times\sin(n\varphi)=0. \tag{6}$$

The corresponding boundary conditions for the phase function are

$$\left[\frac{\partial\psi(\varphi)}{\partial\varphi}+\frac{\partial F}{\partial\varphi}+\frac{\partial}{\partial\xi}\left(\frac{\partial F}{\partial\varphi''}\right)\right]\xi=\frac{L}{2}=0$$
$$\left[\frac{\partial F}{\partial\varphi''}\right]\xi=\frac{L}{2}=0. \tag{7}$$

Under the corresponding boundary conditions, the equation for the amplitude function takes the form

$$\left(1+\frac{5\beta}{\gamma}(\varphi')^2-\frac{\beta}{\gamma}\varphi''\right)R-R^3+\left(1+T\varphi'-(\varphi')^2\right)R$$
$$-K\,R^{n-1}\left(1+\cos(n\varphi)\right)=0. \tag{8}$$

The boundary conditions for the amplitude function are expressed as

$$\left[\frac{\partial\psi(R)}{\partial R}+\frac{\partial F}{\partial R}+\frac{\partial}{\partial\xi}\left(\frac{\partial F}{\partial R''}\right)\right]\xi=\frac{L}{2}=0,$$
$$\left[\frac{\partial F}{\partial R''}\right]\xi=\frac{L}{2}=0. \tag{9}$$

Taking into account expressions (7) and (9), the final boundary conditions for $\xi\geq 0$ are

$$\left[2\varphi'-T-\frac{12\beta r}{\gamma}\left(\frac{R'}{R}\right)^2\right]\varphi'+\frac{12\beta r}{\gamma}\frac{R'}{R}\varphi''=0,$$
$$\left[\varphi''+\frac{2R'}{R}\varphi'\right]=0 \tag{10}$$

and

$$\left[-\frac{\alpha R}{r}+\left(2+\frac{6\beta r}{\gamma}(\varphi')^2\right)\right]R''=0,$$
$$\left[R''-R\,(\varphi')^2\right]=0. \tag{11}$$

These conditions ensure the physical consistency of the finite-size crystal model and correctly describe the influence of surface energy.

Dynamic-regime maps were constructed using recurrence relations of the form

$$x_{n+1}=f(x_n,y_n), \tag{12}$$

$$y_{n+1}=g(x_n,y_n), \tag{13}$$

where the function $f(x_n,y_n)$ describes the behavior of the amplitude R of the IC wave or its derivative R', while the function $g(x_n,y_n)$ describes the behavior of the phase φ or its derivative φ'.

The resulting two-dimensional mapping depends on the parameters $a=K$ and $b=T$. The choice of these parameters is physically justified because T characterizes the strength of long-range interactions, while K determines the strength of anisotropic interactions responsible for modulation distortion and the onset of chaos.

The algorithm used to construct the dynamic-regime maps is based on periodicity convergence. The last element of a numerical sequence is sequentially compared with all preceding elements. If the last value λ coincides with $\lambda-1$, the system is considered to have period 1, corresponding to a limit point. Higher periodicities are identified analogously.

This approach allows visualization of periodic, quasiperiodic, and chaotic regimes in the control-parameter plane (K,T) and provides a direct comparison with Lyapunov-exponent maps and Fourier spectra.

The influence of surface energy on the dynamics of the IC superstructure was investigated using the system of differential equations (8)–(9) together with the boundary conditions (10)–(11), allowing analysis of transitions between different IC states and the commensurate phase.

3. Results and discussion

Using numerical simulation, we investigated the influence of the anisotropic interaction parameter K on the transition of the incommensurate superstructure from periodic to chaotic dynamics. Figure 1 shows the Fourier spectra of the amplitude function $R(\xi)$ calculated for fixed $T=1.0$ and $n=3$ at different values of K. The Fourier transform was applied to the spatial profile of the order-parameter amplitude. At low K, the spectra contain a limited number of pronounced peaks, which correspond to a sinusoidal modulation regime. With increasing K, additional harmonics appear, indicating distortion of the incommensurate wave. At $K=1.5$, the spectrum broadens and becomes irregular, which indicates the transition to a chaotic regime.

Figure 2 presents the dependence of the Lyapunov exponents on the parameter K at a fixed value of $T=1$, which characterizes the stability of the incommensurate superstructure. This value of T was selected following the rationale provided in [8], namely that it corresponds to the maximum

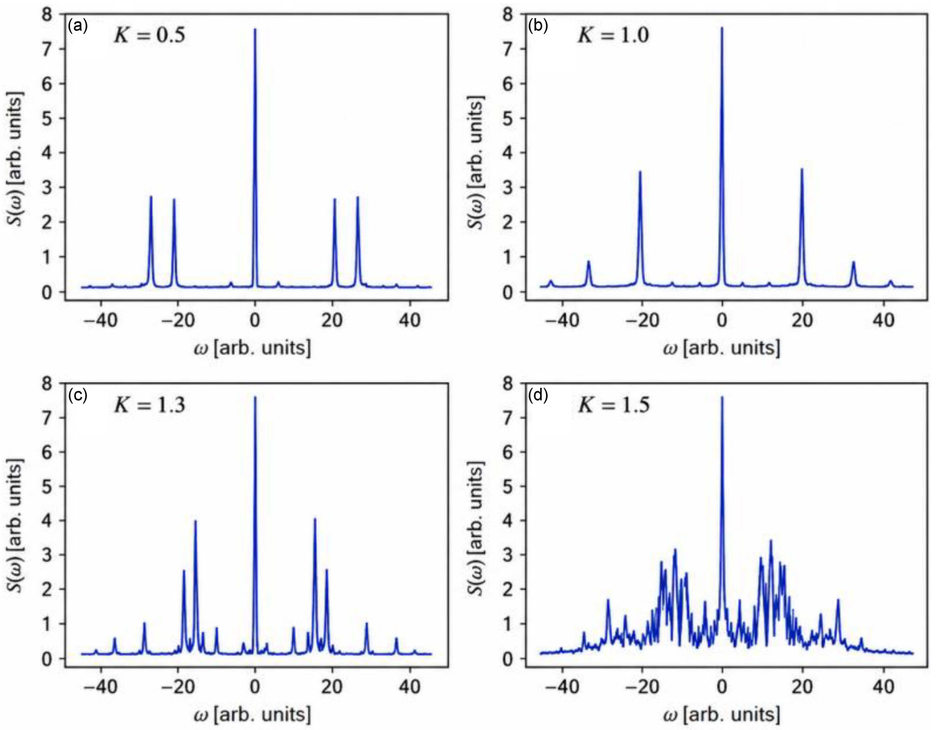

Fig. 1. Fourier spectra of the amplitude function $R(\xi)$ for different values of the anisotropic interaction parameter K at a fixed long-range interaction parameter $T = 1.0$ and $n = 3$: (a) $K = 0.5$, (b) $K = 1.0$, (c) $K = 1.3$, (d) $K = 1.5$.

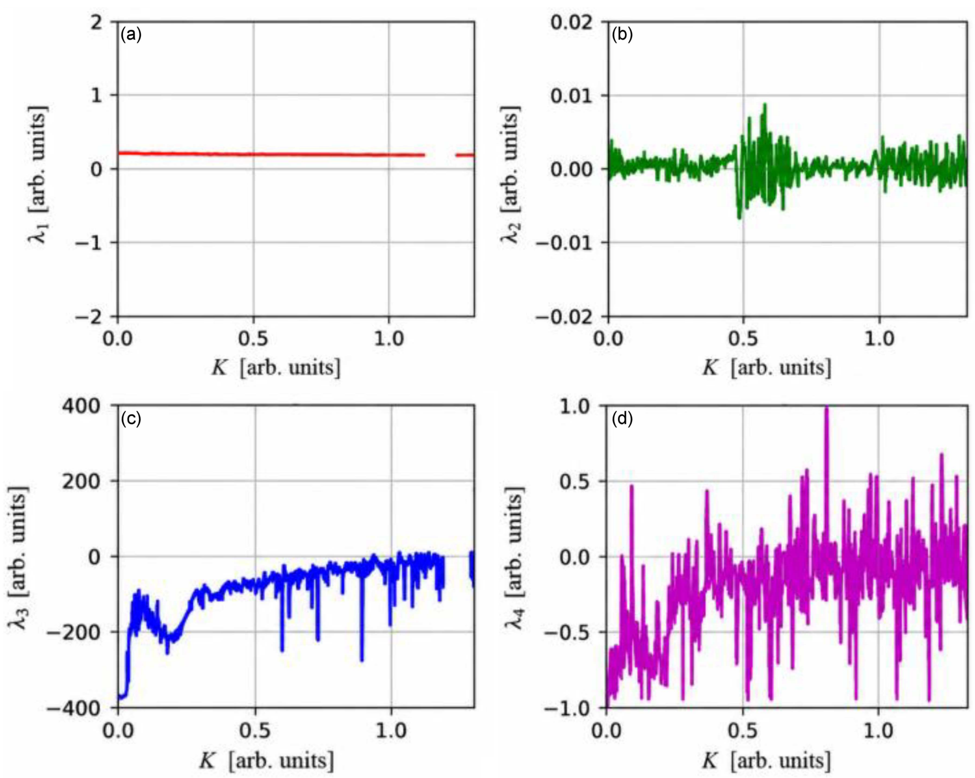

Fig. 2. Dependence of the Lyapunov exponents λ_i on the anisotropic interaction parameter K (Dzyaloshinskii–Lifshitz anisotropy) with fixed long-range interaction parameter $T = 1.0$ and unit-cell multiplication factor $n = 3$. The transition from a strange attractor with one positive Lyapunov exponent to a hyperchaotic regime with two positive Lyapunov exponents occurs near $K \approx 1.2$. Results were obtained by numerical integration of (4)–(5) using the BDF method.

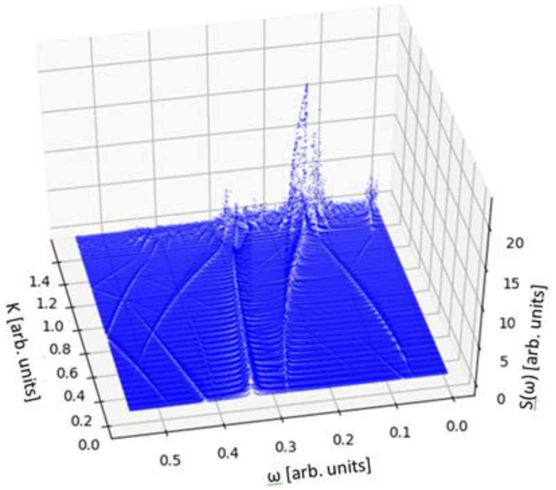

Fig. 3. Fourier spectra of the amplitude oscillations of the incommensurate (IC) superstructure as a function of the anisotropic interaction parameter K for $n = 3$. Each curve corresponds to a fixed value of K in the range $0.2 \leq K \leq 1.6$ with a step $\Delta K = 0.02$. The Fourier transform was calculated from the spatial dependence of the amplitude function $R(\xi)$. The increase in higher harmonics and the broadening of the spectra for $K > 1.2$ indicate the transition from the sinusoidal regime to the solitonic and hyperchaotic states.

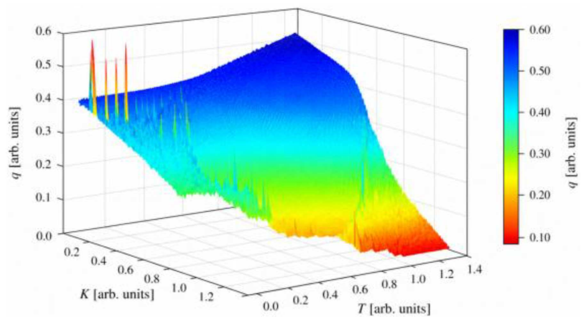

Fig. 4. Dependence of the incommensurate (IC) modulation wave vector q on the long-range interaction parameter T and the anisotropic interaction parameter K (Dzyaloshinskii–Lifshitz anisotropy) for $n = 3$. The increase in T leads to an increase in q and a reduction of the modulation wavelength, while increasing K causes a decrease in q, corresponding to the transition from the sinusoidal regime to the solitonic and stochastic states of the IC superstructure. The color scale represents the magnitude of q in arbitrary units.

value of the long-range interaction force. The examined phase space with dimensionality $n = 3$ for $K < 1.0$ is characterized by a strange attractor with a single positive Lyapunov exponent $(+, -, -, -)$. Therefore, the incommensurate phase in the sinusoidal regime may be regarded as a phase characterized by a strange attractor with a limit cycle.

It is known that with the emergence of higher harmonics in the incommensurate superstructure and the pinning of the latter by defects in the crystal structure, a transition from the sinusoidal to the solitonic regime occurs. The solitonic regime is marked by the formation of long-period commensurate phases and the emergence of a chaotic phase during transitions between such commensurate phases. This may give rise to a condition referred to as hyperchaos $(+, +, -, -)$, characterized by two positive Lyapunov exponents. According to our analysis, this condition is realized for $K > 1.2$ (see Fig. 2). This behavioral scenario is further confirmed by the Fourier spectra diagram shown in Fig. 3.

The modulation wave vector q characterizes the spatial periodicity of the incommensurate superstructure. It determines the modulation wavelength according to $L = 2\pi/q$ and describes the deviation of the structure from the commensurate state. The temperature dependence $q(T)$ reflects the evolution of the modulation period during phase transitions between the parent, incommensurate, and commensurate phases.

To begin, we consider the variation of the incommensurability wave vector within the range 0–1.2. This range of control parameters T and K was chosen based on the results from [9], where a transition to a chaotic state was observed in the Lyapunov exponent profiles ($K \geq 1.2$). It should also be noted that in [8], to realize the minimum of the effective potential, the parameter T for the incommensurate (IC) phase was set to 1. At small values of T and K, as reported in [10], a transition to an incipient (weakly developed) chaotic regime was observed. This region of T and K is associated with the nucleation of the IC superstructure. Figure 4 presents the phase diagram of the IC modulation wave vector as a function of T and K. During the onset of the IC superstructure, an increase in the long-range interaction (parameter T) leads to an increase in the magnitude of the IC wave vector, which reflects a reduction in the modulation wavelength.

Such behavior of q indicates that in spatial regions of correlated motion of tetrahedral groups [11], the modulation wavelength is shorter than at the stage of a fully formed IC superstructure. Under these conditions, upon increasing the anisotropic interaction (increasing K), one identifies a domain where an incipient chaotic state emerges, accompanied by sharp spikes in q that exist within a rather narrow interval of the parameters T and K (Fig. 4).

Further variation of T and K is characterized by a monotonic increase in q at fixed K with increasing T and a monotonic decrease in q at fixed T with increasing K. As is known [1], in the IC phase, the magnitude of the modulation wave vector decreases upon cooling (and thus with increasing anisotropic

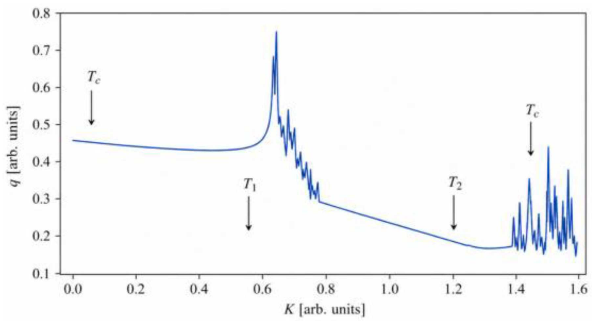

Fig. 5. Evolution of the incommensurate (IC) modulation wave vector q as a function of the anisotropic interaction parameter K at fixed long-range interaction parameter $T = 1.0$ for $n = 3$. The characteristic points indicate the sequence of phase transformations: T_i — transition into the IC phase; T_1 — onset of the solitonic regime; T_2 — onset of the stochastic regime; T_c — transition into the commensurate phase. The decrease in q with increasing K corresponds to an increase in the modulation wavelength and reflects the transition from the sinusoidal regime to the solitonic and stochastic states of the IC superstructure.

interaction K), which indicates an increase in the modulation wavelength. In our case, an increase in the IC modulation period (a decrease in q) is also observed (Figs. 4 and 5).

According to Fig. 4, under a linear increase in the parameters T and K, there exists a range in which an increase in T is accompanied by a decrease in the wave vector of the IC superstructure. We infer that as the number of harmonics of the IC modulation grows, the superstructure undergoes a transition from a sinusoidal to a soliton regime, which effectively reduces T while enhancing K. Further variations of K and T give rise to a chaotic response of q, signalling a transition of the system to a stochastic regime of the IC superstructure and the emergence of a chaotic phase. In summary, the parameters T and K — governing the long-range and anisotropic interactions, respectively — provide, to first order, an adequate description of the behavior of the IC modulation wave vector and its regimes.

In a first approximation, Fig. 4 suggests that the range $T \in [0, 0.6]$ corresponds to the first incommensurate phase, I_1, where chaotic states manifest as sharp variations of q. With stronger long-range interaction ($T > 0.6$), a second incommensurate phase, I_2, is observed, encompassing all regimes of the IC superstructure; this is corroborated by the analysis of modulation harmonics. Figure 5 shows the evolution of the IC wave vector as a function of the anisotropic interaction K at fixed T corresponding to phase coexistence ($T = 0.6$) and to the single-phase I_1 case ($T = 0.3$). In contrast to I_2, no change of the superstructure regime is observed within I_1 upon increasing K.

A comprehensive and transparent view of the system dynamics is provided by dynamical-regime maps; these are diagrams in the parameter plane with two control parameters on the axes and boundaries delineating regions of distinct dynamical behavior. The constructed maps are consistent with alternative representations, such as Lyapunov-exponent maps or Arnold tongues [12], both of which largely reproduce the information conveyed by dynamical-regime maps.

Based on the dependence of the Lyapunov exponents on the anisotropic interaction K for $n = 3$, a transition to a chaotic state is observed for $K > 1.0$. Accordingly, Fig. 6 presents dynamical-regime maps for variations of the parameters $a = K$ and $b = T$ over the range from -2 to 2. These maps exhibit a larger multiplicity of periodicities when the arguments of the recurrence relations are taken to be the phase increment (φ'). In contrast, when the arguments are the amplitude or its increment, the maps display a sharp transition to a state characterized by growth of the amplitude function and its variations (for $K > 1.5$). It is known that such an increase in the amplitude of the spontaneous strain in crystals $[N(CH_3)_4]_2CuCl_4$ is associated with a transition to a commensurate ferroelastic phase, accompanied by the disappearance of the spatial incommensurate modulation [13]. It should also be noted that these crystals exhibit a single incommensurate phase, the structure of which differs (I_1 and I_2) across different regions of the phase diagram [14].

In the dynamical-regime maps, black color denotes periodicities with period $N > 14$; within this region, periodicities with periods exceeding this threshold may occur. Consequently, this domain can be regarded as a region of possible incommensurate phases with distinct structures. Exiting the black region into the red region signals a transition to the period-1 state.

In constructing the maps, we retained only the first fourteen periodicities (red-1, orange-2, yellow-3, green-4, cyan-5, blue-6, violet-7, and so on; black-$N > 14$ for all remaining cases). White indicates the absence of any periodicity. The lowest-period states (red-1, orange-2, yellow-3, green-4) dominate the dynamical-regime maps (Fig. 6).

From the analysis of the dynamical-regime maps, for $\varepsilon = 0.01$ (the parameter quantifying the mismatch between periodicities) and with the long-range interaction fixed at $T = 1$, we find good agreement with the behavior of the Lyapunov exponents upon varying the anisotropic interaction K. Specifically, (i) two "black" regions are observed, corresponding to the presence of two incommensurate (IC) phases in the adopted color code, and (ii) the IC phase disappears at $K \approx 1.5$. Since the observed periodicities can be associated with lock-ins of the incommensurability wave vector to higher-order commensurate values, the appearance of narrow stability windows for these periodicities

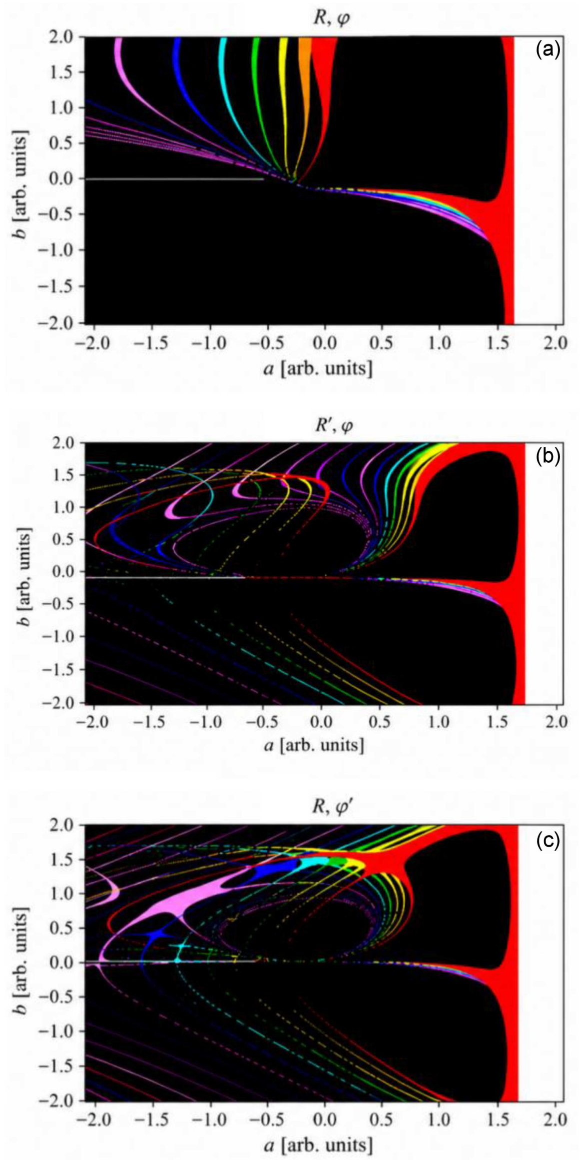

Fig. 6. Map of dynamical regimes in the (a, b) plane for different variables: (a) (R, φ), (b) (R', φ), and (c) (R, φ'). Here, $a = K$ is the anisotropic interaction parameter (Dzyaloshinskii–Lifshitz anisotropy) and $b = T$ is the long-range interaction parameter. The black regions correspond to periodicities with period $N > 14$ and represent possible incommensurate (IC) phases with different internal structures. The transition from the black region to low-period states indicates lock-in transitions into commensurate phases. Calculations were performed for $n = 3$ and $\varepsilon = 0.01$.

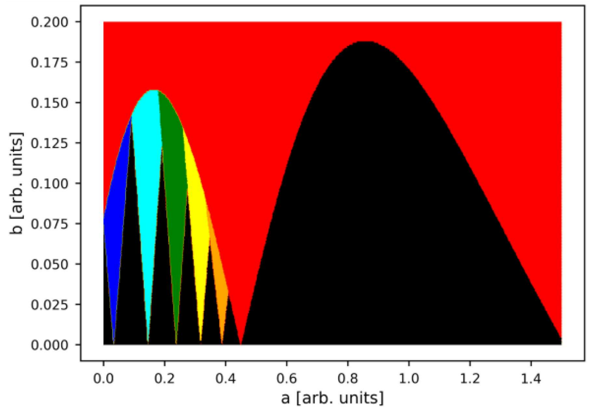

Fig. 7. Two-dimensional map of possible periodicities in the (a, b) plane. Here, $a = K$ is the anisotropic interaction parameter, $b = \varepsilon$ is the interlayer interaction parameter, $n = 3$, and $T = 1$. Different colors indicate the periodicity N of the system: $8 \leq N \leq 14$ (blue), $5 \leq N \leq 7$ (cyan), $3 \leq N \leq 4$ (green), $N = 2$ (yellow), $N = 1$ (red), and chaotic states corresponding to the incommensurate (IC) phase (black). The widths of the periodicity windows decrease with increasing ε.

in the dynamical-regime maps supports the choice of $\varepsilon = 0.01$.

Figure 7 shows the existence map of possible periodicities as a function of the anisotropic interaction K under maximal long-range interaction ($T = 1$). As seen in Fig. 7, increasing ε reduces the width of the periodicity windows. Two K-intervals of chaotic states (IC phases) are also evident and exhibit distinct periodicity dynamics: the first interval, $K = 0$–0.4, contains both period-N states with $N < 14$ and with $N > 14$, whereas the second interval, $K = 0.4$–1.5, features only states with $N > 14$.

Building on the observed evolution of periodicities with the anisotropic interaction, we infer that the crystal hosts a single incommensurate (IC) phase; at $K = 0.4$, there is merely a change of regime of the IC superstructure from sinusoidal to solitonic. According to Fourier-spectrum analyses of the amplitude and phase functions of the IC superstructure [15, 16], the soliton regime is characterized by the presence of multiple periodicities. The dependence of the harmonics of the incommensurability wave vector q on the anisotropic interaction K evidences complex transformations at the sinusoidal–soliton transition near $K = 0.4$, in agreement with previous investigations of related ferroic crystals [17].

To elucidate the processes at $K = 0.4$, we examine two-dimensional dynamical-regime maps for $\varepsilon = 0.01$ (Fig. 6). As shown in Fig. 6, the transition from one chaotic state to another proceeds via a cascade of periodicities. These periodicities govern the behavior of the first IC domain (a chaotic state for $K \approx 0$–0.5). It is known that the appearance of harmonics in the IC modulation drives the transition from a sinusoidal to a soliton regime [15]. If harmonics emerge already within the sinusoidal regime and trigger this transition, then both the sinusoidal and the transitional ranges should exhibit periodicities, while the soliton regime, in the ideal case, should display at least as many periodicities.

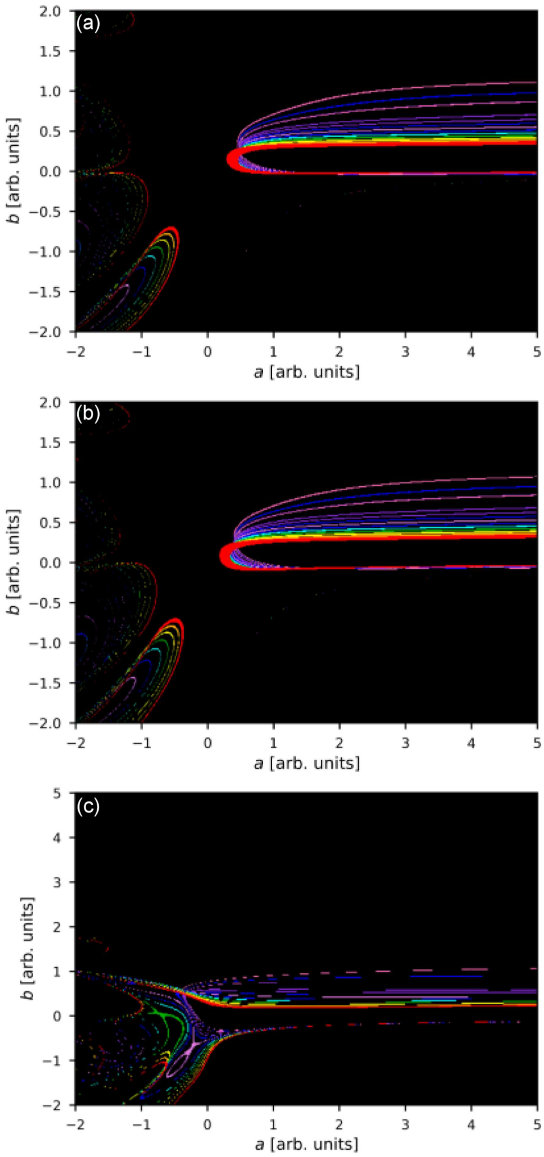

Fig. 8. Dynamical-regime maps in the (a, b) plane for different values of the surface energy E: (a) $E = 0.07$, (b) $E = 0.2$, and (c) $E = 0.7$. Here, $a = K$ is the anisotropic interaction parameter (Dzyaloshinskii–Lifshitz anisotropy) and $b = T$ is the long-range interaction parameter for $n = 3$. The increase in surface energy induces a transformation between two structurally distinct incommensurate (IC) states through an intermediate commensurate phase characterized by low-period states. A further increase in E narrows the stability region of the IC phase and eventually leads to its suppression by the commensurate phase.

The observed black region for increasing K (i.e., $K = 0.5$–1.5), in which no periodicities with $N < 14$ are detected, may be associated with the formation of a chaotic superstructure; this interpretation is supported by the K-dependence of the Lyapunov exponents, which indicates the onset of a chaotic state for $K \geq 1.0$. In light of the maps in Fig. 6, the transition to chaos is driven predominantly by changes in the phase function of the IC state, whereas the amplitude function is responsible for the persistence of periodicities within the first chaotic phase. This interpretation is also consistent with modern studies of nonlinear dynamics and Lyapunov-based characterization of complex systems [18].

To clarify the behavior of the IC superstructure near $K = 0.4$, we further consider the effect of surface energy on the phase state. It is known that surface energy primarily modifies the amplitude of the order parameter and produces a phase shift [12, 19]. Accordingly, we analyze a two-dimensional mapping in which the recurrence relations are formulated for the amplitude R and phase φ of the order parameter. The resulting two-dimensional dynamical-regime maps are presented in Fig. 8.

From experimental studies [12, 14] on the effect of surface energy on the incommensurate (IC) superstructure in $(N(CH_3)_4)_2CuCl_4$ — where the IC wave vector takes the form $q_i = (\frac{1}{3} + \delta)c^*$ (with $n = 3$, $m = 1$) — it is known that surface energy drives a transformation between distinct IC superstructures via an intermediate commensurate (C) phase, which is consistent with previous crystallographic and phenomenological studies [20, 21]. (Here, c^* denotes the reciprocal lattice vector corresponding to the crystallographic c-axis.) A further increase in surface energy narrows the stability interval of the IC phase by raising the transition temperature T_c of the IC–C transition and lowering the transition temperature T_i of the parent IC transition.

An analogous behavior is reflected in the dynamical-regime maps for the present system with $n = 3$. Specifically, when the dependence of the long-range interaction $T = b$ and the anisotropic interaction $K = a$ on the surface energy E is taken into account, varying E induces a transition from one IC state to another through an intermediate commensurate state, which is characterized by the shortest periods (in Figs. 6 and 8, this region corresponds to the color palette from red to violet). A further increase in E progressively narrows the IC domain via concomitant changes in T and K, ultimately filling this region with the commensurate state characterized by the shortest-period periodicities. The obtained phase transformations are also in qualitative agreement with recent investigations of modulated crystal structures and dimensional effects reported in [22, 23].

4. Conclusions

The present study demonstrates that the dynamics of incommensurate superstructures in $(N(CH_3)_4)_2CuCl_4$ with a unit-cell multiplication factor $n = 3$ are governed by the competition between anisotropic interaction K and long-range interaction T.

The physical significance of $n = 3$ is associated with the tripling of the unit cell and the emergence of threefold anisotropy in the thermodynamic potential, which determines the structure of the incommensurate phase and the sequence of phase transitions.

Numerical analysis of Fourier spectra, Lyapunov exponents, modulation wave-vector evolution, and dynamic-regime maps reveals the existence of two structurally distinct incommensurate states within a single IC phase. The first regime corresponds to a sinusoidal modulation with narrow periodicity windows and localized chaotic behavior, while the second regime corresponds to a solitonic and stochastic structure characterized by higher harmonics, broader periodicity distributions, and hyperchaotic dynamics.

The transition between these regimes occurs near $K \approx 0.4$ and is driven by the appearance of additional harmonics of the modulation wave. For $K > 1.2$, the system enters a hyperchaotic state characterized by two positive Lyapunov exponents.

Surface energy significantly modifies the phase behavior by changing the effective anisotropic interaction and shifting the stability interval of the incommensurate phase. Increasing surface energy induces a transition between distinct IC structures through an intermediate commensurate phase and eventually suppresses the IC phase.

These results provide a physically transparent framework for understanding the evolution of incommensurate phases in low-symmetry ferroelastic crystals and clarify the role of anisotropy, long-range interactions, and surface effects in the formation of complex modulated states.

References

[1] H.Z. Cummins, *Phys. Rep.* **185**, 211 (1990).

[2] R. Blinc, B. Žekš, *Adv. Phys.* **21**, 693 (1972).

[3] P. Toledano, V. Dmitriev, *Reconstructive Phase Transitions: In Crystals and Quasicrystals*, World Scientific, Singapore 1996.

[4] S. Sveleba, I. Katerynchuk, I. Karpa, I. Kunyo, V. Rak, O. Yashchyk, in: *Proc. 10th Int. Conf. on Advanced Computer Information Technologies (ACIT 2020)*, IEEE, Deggendorf (Germany) 2020, p. 200.

[5] W.L. McMillan, *Phys. Rev. B* **14**, 1496 (1976).

[6] H. Mashiyama, S. Tanisaki, K. Gesi, *J. Phys. Soc. Jpn.* **50**, 1415 (1981).

[7] G. Ansmann, *Chaos* **28**, 043116 (2018).

[8] F. Bouchet, S. Gupta, D. Mukamel, *Physica A* **389**, 4389 (2010).

[9] S. Sveleba, I. Katerynchuk, I. Kunyo, I. Karpa, Ya. Shmygelskyi, *Electron. Inf. Technol.* **12**, 82 (2019) (in Ukrainian).

[10] S. Sveleba, I. Katerynchuk, I. Karpa, I. Kunyo, V. Rak, O. Yashchyk, in: *2020 10th Int. Conf. on Advanced Computer Information Technologies (ACIT)*, IEEE, Deggendorf (Germany) 2020, p. 200.

[11] S. Sveleba, I. Katerynchuk, I. Kuno, I. Karpa, O. Semotiuk, *Mol. Cryst. Liq. Cryst.* **752**, 95 (2022).

[12] G. Benettin, L. Galgani, A. Giorgilli, J.-M. Strelcyn, *Meccanica* **15**, 9 (1980).

[13] I.M. Kunyo, I.V. Karpa, S.A. Sveleba, I.M. Katerynchuk, "Dimensional Effects in Dielectric Crystals $[N(CH_3)_4]_2MeCl_4$ (Me = Cu, Zn, Mn, Co) with an Incommensurate Phase", Ivan Franko National University of Lviv, Lviv 2019, p. 220 (in Ukrainian).

[14] S. Sveleba, I. Katerynchuk, I. Kuno, I. Karpa, O. Semotiuk, V. Brygilevych, *Computat. Probl. Electr. Eng.* **10**, 28 (2020).

[15] S. Lynch, *Dynamical Systems with Applications Using Python*, Springer, Cham 2018.

[16] S. Sveleba, O. Semotyuk, I. Katerynchuk, I. Kunyo, I. Karpa, Yu. Pankivskyi, *Acta Phys. Pol. A* **114**, 791 (2008).

[17] V. Kapustianyk, Z. Czapla, S. Dacko, O. Czupinski, V. Rudyk, R. Serkiz, S. Sereda, S. Semak, *Acta Phys. Pol. A* **127**, 791 (2015).

[18] A. Pikovsky, A. Politi, *Lyapunov Exponents: A Tool to Explore Complex Dynamics*, Cambridge University Press, 2016.

[19] P. Bak, *Rep. Prog. Phys.* **45**, 587 (1982).

[20] J. Hlinka, P. Márton, *Phys. Rev. B* **74**, 104104 (2006).

[21] J.M. Pérez-Mato, S.V. Gallego, L. Elcoro, M.I. Aroyo, *J. Phys. Condens. Matter* **24**, 163201 (2012).

[22] A.A. Gaydamaka, S.V. Rashchenko, *Acta Crystallograph. B* **80**, 315 (2024).

[23] D. Savytskii, T. Tataryn, U. Bismayer, *Acta Phys. Pol. A* **117**, 78 (2010).